Monte Carlo studies of $d = 2$ Ising strips with long-range boundary fields

2000 J. Phys.: Condens. Matter 12 2701

(http://iopscience.iop.org/0953-8984/12/12/311)

J. Phys.: Condens. Matter **12** (2000) 2701–2723. Printed in the UK PII: S0953-8984(00)09794-0

Monte Carlo studies of $d = 2$ Ising strips with long-range boundary fields

E V Albano†, K Binder‡ and W Paul‡

† INIFTA, Universidad Nacional de La Plata, CONICET, CIC, CC 16 Suc. 4, (1900) La Plata, Argentina

‡ Institut für Physik, Johannes-Gutenberg-Universität Mainz, Staudinger Weg 7, D-55099 Mainz, Germany

Received 23 November 1999, in final form 25 January 2000

Abstract. A two-dimensional Ising model with nearest-neighbour ferromagnetic exchange confined in a strip of width L between two parallel boundaries is studied by Monte Carlo simulations. 'Free' boundaries are considered with unchanged exchange interactions at the boundary but long-range boundary fields of the form $H(n) = \pm h[n^{-3} - (L - n + 1)^{-3}]$, where $n = 1, 2, \ldots, L$ labels the rows across the strip. In the case of competing fields and $L \to \infty$, the system exhibits a critical wetting transition of a similar type as in the well studied case of short-range boundary fields. At finite L, this wetting transition is replaced by a (rounded) interface localization–delocalization transition at $T_c(h, L)$. The order parameter profiles and correlation function $G_{\parallel}(n, r)$, where r is a coordinate parallel to the boundaries of the strip, are analysed in detail. It is argued that for $T \geqslant T_c(h, L)$ the order parameter profile is essentially a linear variation across the strip, i.e. the width w varies as $w \propto L$, unlike the case in $d = 3$ where $w \propto L^{1/2}$ is the short-range case and $w \propto \ln L$ in the case of the n^{-3} boundary potential holds. The parallel correlation length $\xi_{\parallel}$ scales as $\xi_{\parallel} \propto L^2$ as for the short-range case. In addition to this case of competing boundary fields, also the case where both boundaries are sources of fields of the same sign is studied, which then compete with a uniform bulk field such that a capillary condensation transition occurs. The data obtained are consistent with the Kelvin equation as in the case of the short-range surface fields.

1. Introduction

The interplay of finite-size effects and surface behaviour in systems confined by boundaries has found much interest recently [1–57]. In particular, wetting transitions [58–98] become significantly modified in confined geometry [31, 35, 37, 50–53, 57]. This influence on wetting phenomena results from the constraining effect that external boundaries have on interfacial fluctuations: in fact, understanding the interfacial profile and related correlations is an interesting problem in itself [7, 9, 11, 14, 19, 47, 48, 90–98].

A particularly useful model to study such questions is the two-dimensional Ising lattice exposed to boundary fields [1, 3–8, 29–31, 33, 37, 40, 44, 47, 48]. The interest in this model is not so much due to experimental applications (possible e.g. via adsorption on regularly stepped surfaces [31]) but due to the availability of exact calculations, at least in certain limiting cases [27, 60–63]. Therefore almost all previous work (with the exception of Privman and Švrakić [81] who considered wall potentials of $1/r$ type) has considered short-range forces due to the boundaries. It is known [73, 74, 79], however, that long-range forces modify the wetting behaviour significantly, and in fact for many physical problems, such as adsorption on stepped surfaces where electronic charge distribution at steps causes the occurrence of dipolar

0953-8984/00/122701+23$30.00

potentials, the choice of long-range forces would be more realistic [97] than their short range counterparts [96].

In the present paper we hence consider a nearest-neighbour Ising ferromagnet on $L \times M$ square lattices (with $M \gg L$) and on the two boundaries (of length M) we apply long-range boundary fields, which depend on the distance n of a lattice site from the boundary proportional to n^{-3}. Both the case of competing fields (opposite sign), where for temperatures T sufficiently less than the critical temperature T_c an interface running parallel to the boundaries is stabilized, and the case where both boundary fields have the same sign are considered. Then a phase transition (capillary condensation) occurs at a suitable bulk field of a sign opposite to the sign of the boundary fields [8, 10, 29, 30, 41–43, 50, 56]. Here we are interested in comparing both this capillary condensation transition and the interface localization–delocalization transition that occurs for competing boundary fields [31, 33, 35, 37, 38, 44, 50–53, 57] with their short-range counterparts. Note that there is also a rich knowledge on boundary effects right at the bulk T_c [1, 3–6, 15, 40, 46] that is useful in the present context.

In the following section we briefly review the known results pertinent for the present work, while in section 3 we describe our results for competing boundary fields. Section 4 contains our data for capillary condensation induced by long-range boundary fields, while section 5 summarizes our conclusions.

2. Theoretical background

2.1. Ising model

We consider an Ising ferromagnet on the square lattice

$$\mathcal{H} = -J \sum_{\langle i,j \rangle} S_i S_j - H \sum_i S_i - \sum_n H(n) \sum_{i \epsilon n} S_i \tag{1}$$

where J is the nearest-neighbour exchange, the sum $\langle i, j \rangle$ is extended once over all nearest-neighbour bonds and H is a uniform field that acts on all spins.

Choosing an $L \times M$ geometry with periodic boundary conditions in the x-direction, figure 1, we have free boundary conditions in the y-direction, where we label successive layers by the index n, and apply fields due to the free boundaries adjacent to the spins in layers $n = 1$ and $n = L$, respectively. While in previous work typically short-range boundary fields were used, either of symmetric strength [30, 56]

$$H(n) = h[\delta_{1n} + \delta_{Ln}] \qquad n = 1, \ldots, L \tag{2}$$

or competing boundaries [31, 33, 37]

$$H(n) = h[-\delta_{1n} + \delta_{Ln}] \qquad n = 1, \ldots, L \tag{3}$$

in the present work we choose a potential that reduces to an n^{-3} potential for $L \to \infty$. In the case of competing boundaries we take

$$H(n) = h[-n^{-3} + (L - n + 1)^{-3}] \qquad n = 1, \ldots, L \tag{4}$$

while in the case of symmetric boundaries we take

$$H(n) = h[n^{-3} + (L - n + 1)^{-3}] \qquad n = 1, \ldots, L. \tag{5}$$

Note that in the limit $h \to \infty$ equation (2) reduces to the (++) fixed spin boundary condition while equation (3) reduces to the (−+) boundary condition (for $h > 0$), widely studied in the literature (e.g. [48]).

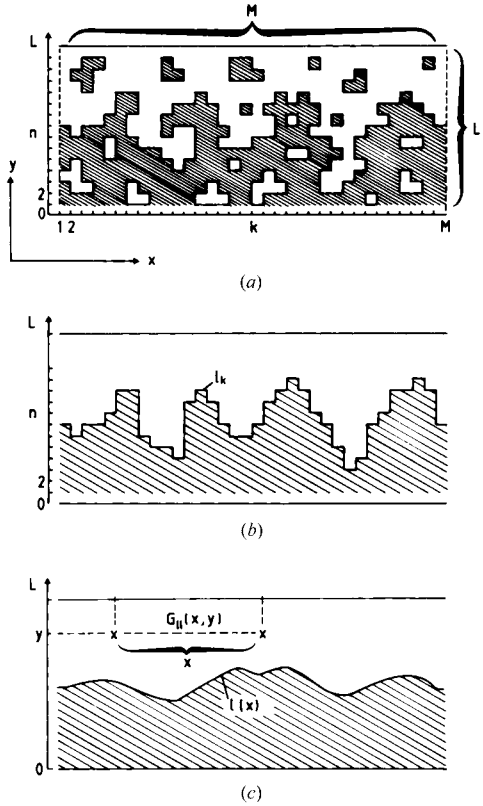

Figure 1. Schematic configuration of an Ising $L \times M$ square lattice (a) with competing boundary fields described by equation (3), contrasted with a solid-on-solid (SOS) configuration of an interface (b), as well as the corresponding continuum ('capillary wave') model of the interface (c). In the x-direction, always periodic boundary conditions are applied. If a spin at site $y = n, x = k$ is oriented negative, then the square for which this site is the lower left corner has been shaded. In part (c), the definition of the correlation function $G_{\|}(x, y)$ between spins at two sites (marked by crosses) with the same y-coordinate a distance x apart in the x-direction is indicated.

2.2. SOS limit and exact results

It is well known that the Ising model with competing boundaries (equation (3)) for $T \to 0$ reduces to the solid-on-solid (SOS) model, where all bulk fluctuations (i.e., bubbles and holes if one interprets the Ising magnet as a lattice gas, cf figure 1(a)) are suppressed, and overhangs of the interface contour also are excluded (figure 1(b)). The only degree of freedom then is the local height variable ℓ_k, and the bulk term of the Hamiltonian equation (1) reduces to (for $H = 0$)

$$\mathcal{H}_{SOS} = -2J \sum_k |\ell_{k+1} - \ell_k|. \tag{6}$$

The great simplification that equation (6) amounts to is that via equation (6) the original two-dimensional Ising problem has been reduced to a quasi-one-dimensional Hamiltonian, which is readily solved by transfer matrix methods [99]. Here we are interested in a correlation function of spins displaced in a direction parallel to the boundaries, where $i = (k, n = y)$,

$j = (k + x, n = y)$,

$$G_{\parallel}(x, y) = \langle S_i S_j \rangle - \langle S_i \rangle \langle S_j \rangle \tag{7}$$

and the correlation length $\xi_{\parallel}$ which describes its asymptotic decay, $G_{\parallel}(x, y) \propto \exp(-x/\xi_{\parallel})$ as $x \to \infty$. For the Ising problem with $(-+)$ boundary conditions in the SOS limit it has been shown [47, 99]

$$1/\xi_{\parallel} = \ln\{[\cosh(2J/k_BT) - \cos(2\pi/L)]/[\cosh(2J/k_BT) - \cos(\pi/L)]\} \tag{8}$$

which for large L reduces to

$$\xi_{\parallel} \approx \frac{2[\cosh(2J/k_BT) - 1]}{3\pi^2} L^2. \tag{9}$$

For the $(-+)$ boundary condition also the magnetization profile $m(y) = \langle S_i \rangle$ across the interface is known in the SOS limit [48, 99]

$$m(y) = (2y/L - 1) + \pi^{-1} \sin[\pi(2y/L - 1)]. \tag{10}$$

Defining a width of the interfacial profile W from the second moment [95],

$$W^2 = 2 \int \mathrm{d}y (y - y_0)^2 (\mathrm{d}m/\mathrm{d}y) \Big/ \int \mathrm{d}y (\mathrm{d}m/\mathrm{d}y) \tag{11}$$

where y_0 is the midpoint of the profile, one finds [48]

$$W = (L + 1)(1/6 - 1/\pi^2)^{1/2} \approx 0.2556(L + 1). \tag{12}$$

From equations (10) and (12), one can already see that the width of the interface is of the same order as the strip width itself, W scales linearly with L, which means that the local position ℓ_k of the interface in figure 1(b) explores the full region of the strip and is not localized near the midpoint ($y_0 = (L + 1)/2$ if L is odd) of the profile.

Using the transfer matrix solution for the Ising model with $(-+)$ boundary condition [100] the correlation length $\xi_{\parallel}$ [47] and the profile $m(y)$ [48] can be worked out at arbitrary temperatures. In particular, one finds for $T = T_c$

$$\xi_{\parallel}^{-1} \approx \pi/L - \pi/(\sqrt{2}L^2) + \cdots \tag{13}$$

while for $T < T_c$ and $L \to \infty$ [27, 47]

$$\xi_{\parallel}^{-1} = [3\pi^2(2\sigma/k_BT)]L^{-2} \tag{14}$$

σ/k_BT being the interfacial stiffness. Since in the SOS limit $\sigma/k_BT = \cosh(2J/k_BT) - 1$, equation (14) reduces to equation (9) for T for below T_c (numerical analysis shows [47] that actually equation (9) approximates the Ising results accurately for $T \leqslant 0.6\ T_c$.)

The sigmoidal shape of the magnetization profile, equation (10), gradually flattens [48] as the temperature is raised, and right at T_c the profile is known exactly from conformal invariance [40] for $L \to \infty$,

$$m(y) = -A\left[\frac{L}{\pi} \sin\left(\frac{\pi y}{L}\right)\right]^{-1/8} \cos\left(\frac{\pi y}{L}\right) \tag{15}$$

where A is a constant. Equation (15) implies again $W \propto L$, the constant of proportionality being similar to that of equation (12) [48].

However, we emphasize that the $d = 2$ Ising model with $(-+)$ boundary condition (corresponding to $h \to \infty$ in equation (3)) does not exhibit any interface localization–delocalization transition: only for $h/J < 1$ does the corresponding semi-infinite Ising model have a wetting transition [60] at $h_c(T)$ given by

$$\exp(2J/k_BT)[\cosh(2J/k_BT) - \cosh(2h_c/k_BT)] = \sinh(2J/k_BT). \tag{16}$$

At the wetting temperature $T_w(h)$ (the inverse function of $h = h_c(T)$ given by equation (16)) the magnetization profile is particularly simple, namely linear [37]

$$m(y) = m_b(-1 + 2y/L) \tag{17}$$

except in the immediate vicinity of the boundaries. In equation (17), m_b is the bulk magnetization of the Ising model at $T = T_w(h)$. From equation (17) we recognize that the width W (equation (11)) becomes $W = L/\sqrt{6}$.

2.3. Continuum theory: results for the capillary wave Hamiltonian

We now turn to the description of the confined interface in terms of the capillary wave Hamiltonian (see figure 1(c))

$$\mathcal{H}(\ell) = \int_0^M \mathrm{d}x \left\{ \frac{\sigma_{\mathrm{eff}}}{2} \left[\frac{\mathrm{d}\ell(x)}{\mathrm{d}x} \right]^2 + V_{\mathrm{eff}}[\ell(x)] \right\}. \tag{18}$$

Here $\sigma_{\mathrm{eff}}/k_BT$ is the interfacial stiffness (for simplicity we take for σ_{eff} the same value as for a free unconfined interface between coexisting phases in the bulk, ignoring a possible position dependence $\sigma(\ell)$ [85, 86]), and $V_{\mathrm{eff}}(\ell)$ is an effective potential acting on the interface position due to the confining boundaries. According to mean field theory, $\ell(x)$ would be weakly fluctuating and then $V_{\mathrm{eff}}(\ell)$ can be expanded around the midpoint position $\ell = L/2$ in the strip [44, 53]. This yields, omitting constant terms ($u(x) = \ell(x) - L/2$)

$$\mathcal{H}(u) = \int_0^M \mathrm{d}x \left\{ \frac{\sigma_{\mathrm{eff}}}{2} \left[\frac{\mathrm{d}u(x)}{\mathrm{d}x} \right]^2 + \frac{1}{2} \frac{\partial^2 V_{\mathrm{eff}}}{\partial \ell^2} \bigg|_{\ell = L/2} u^2 \right\}. \tag{19}$$

Fourier decomposition of the local interface position $u(x)$ and use of the equipartition theorem yields for the mean square value of the Fourier component $u(q)$ [53, 79, 84]

$$\langle |u(q)|^2 \rangle^{-1} = \frac{\sigma_{\mathrm{eff}}}{k_BT} (q^2 + \xi_\parallel^{-2}) \tag{20}$$

where the parallel correlation length for interfacial fluctuations is given by

$$\xi_\parallel = [\sigma / \partial^2 V_{\mathrm{eff}}(\ell)/\partial \ell^2|_{\ell = L/2}]^{1/2}. \tag{21}$$

For short-range surface fields as given in equation (3) one employs an effective potential decaying exponentially with ℓ [44, 53, 79, 84], a_0, b_0 and κ being constants,

$$\begin{aligned} V_{\mathrm{eff}}(\ell) = a_0 \frac{T - T_w(h)}{T_w(h)} [\exp(-\kappa \ell) + \exp(-\kappa(L - \ell))] \\ + b_0 [\exp(-2\kappa L) + \exp(-2\kappa(L - \ell))] \end{aligned} \tag{22}$$

which approximates the exact behaviour [101] $V_{\mathrm{eff}}(\ell) \sim \delta(\ell) + \delta(L - \ell)$ for $\ell \gg \kappa$ and then

$$\frac{\partial^2 V_{\mathrm{eff}}(\ell)}{\partial \ell^2} \bigg|_{\ell = L/2} = 2 \exp[-\kappa L/2] \kappa^2 \left[a_0 \frac{T - T_w(h)}{T_w(h)} + 4 b_0 \exp(-\kappa L/2) \right] \tag{23}$$

and then we have for $T > T_c(L) = T_w(h)\{1 - 4b_0 \exp(-\kappa L/2)\}$ a correlation length that diverges exponentially with L as $L \to \infty$,

$$\xi_\parallel \propto \{[T - T_c(L)]/T_w(h)\}^{-1/2} \exp(\kappa L/4). \tag{24}$$

On the other hand, for a long-range potential of the form $H(y) = h[-y^{-\zeta} + (L - y)^{-\zeta}]$ (cf equation (4)) the effective potential $V_{\mathrm{eff}}(\ell)$ becomes

$$V_{\mathrm{eff}}(\ell) = \int_0^L \mathrm{d}y H(y) m(y) \tag{25}$$

where one writes for the interfacial profile $m(y) = \tanh[(L/2 + u)/w_0]$, with w_0 being the 'intrinsic width' of the interface. This yields (for $\zeta = 3$)

$$\left.\frac{\partial^2 V_{\text{eff}}(\ell)}{\partial \ell^2}\right|_{\ell=L/2} \propto hL^{-4} \qquad \xi_\parallel \propto L^2. \tag{26}$$

Thus in this case mean-field theory predicts a much weaker increase of $\xi_\parallel$ with L than equation (24), namely an increase with the square of the strip width.

However, it must be emphasized that the mean-field result, equation (24), is completely wrong in the two-dimensional case [27, 44] although it works at least qualitatively for $d = 3$ dimensions [51–53, 96]. Rather than an exponential variation of $\xi_\parallel$ with L, one finds a power law as in equation (26), for a boundary potential as given in equation (3)

$$\xi_\parallel \propto L^2. \tag{27}$$

Equation (27) applies for temperatures above a 'pseudocritical' temperature $T_c(L)$ with $T_w - T_c(L) \propto L^{-1}$; below $T_c(L)$ one has no true symmetry-broken phase but rather domains (of length $\ell_{\text{domain}} \propto \exp(\text{const} \times L)$) alternate where the interface is either bound to the lower boundary or to the upper boundary [44]. This prediction reflects the fact that the Ising strip is a quasi-one-dimensional system with short-range interactions and hence cannot show a true phase transition [102]. One can interpret equation (27) from the fact that the meandering interface (figure 1(b), (c)) creates at a distance ℓ from a wall an effective *entropic* repulsive interaction [68, 73], in $d = 2$ dimensions

$$V_{\text{entropic}}(\ell) \propto k_B T \ell^{-2}. \tag{28}$$

Using equation (28) in the mean-field formula, equation (21), one would recover the correct result, equation (27).

Being interested also in the problem of capillary condensation, where $H > 0$ in equation (1), we ask how $\xi_\parallel$ behaves in the presence of nonzero bulk field H. For the short-range case, the correlation length shows a scaling [44, 45]

$$\xi_\parallel \propto L^2 \tilde{\xi}(LH^{1/3}). \tag{29}$$

Note that for large H the L-dependence cancels out from equation (29), since the scaling function $\tilde{\xi}(\zeta)$ behaves as $\tilde{\xi}(\zeta) \sim \zeta^{-2}$, and hence $\xi_\parallel \propto H^{-2/3}$. The typical configurations then consist of flat droplets of negative magnetization attached to the walls with a lateral extension $\xi_\parallel$ and a vertical extension $\xi_\perp \propto \bar{\ell} \propto H^{-1/3}$ [68, 73]. Such configurations have indeed been observed in recent simulations [56].

Wetting in $d = 2$ in the presence of long-range forces has been discussed by Kroll and Lipowsky [65] and by Fisher and Huse [69]. For complete wetting, the effective interface potential is

$$V_{\text{eff}}(\ell) = -H\ell + b\ell^{-\delta} \tag{30}$$

b being a suitable constant ($b > 0$). For $\delta > 2$ the second term on the right-hand side of equation (30) is irrelevant, the entropic repulsion (equation (28)) dominates and one still has the same behaviour for $\xi_\parallel$, $\xi_\perp$ and the mean distance of the interface from the wall as in the short-range case

$$\xi_\perp \propto \bar{\ell} \propto H^{-1/3} \qquad \xi_\parallel \propto \xi_\perp^2 \propto H^{-2/3} \qquad H \to 0. \tag{31}$$

On the other hand, for $\delta < 2$ the long-range potential in equation (30) is relevant and the simple scaling $\xi_\parallel \propto \bar{\ell}^2$ is no longer valid since [69, 73]

$$\bar{\ell} \propto H^{-1/(\delta+1)} \qquad \xi_\parallel \propto H^{-(\delta+2)/[2(\delta+1)]} \qquad \xi_\perp \propto H^{-(\delta+2)/[4(\delta+1)]}. \tag{32}$$

Thus for $\delta < 2$ the diffuseness of the interface (which is measured by $\xi_\perp$) is much smaller (for $H \to 0$) than the average distance $\bar{\ell}$ from the wall, unlike the short-range case where both lengths are predicted to be always of the same order of magnitude.

If we assume that equation (20) remains valid, if one simply uses the correct value of $\xi_\parallel$, we can calculate the mean square displacement of the interface for finite M as follows

$$s^2 = \langle u^2(x)\rangle = \sum_q \langle |u(q)|^2\rangle = \frac{1}{2\pi}\int_{2\pi/M}^{2\pi/a} \mathrm{d}q\, \langle |u(q)|^2\rangle \tag{33}$$

where a is a short-wavelength cutoff (in the extreme case, a is the lattice spacing). Combining equations (20) and (33) then yields

$$s^2 = \frac{\xi_\parallel}{2\pi\sigma_{\mathrm{eff}}}\left[\tan^{-1}\frac{2\pi\xi_\parallel}{a} - \tan^{-1}\frac{2\pi\xi_\parallel}{M}\right]. \tag{34}$$

We are interested in the limit $\xi_\parallel \gg a$, of course, where $\tan^{-1}(2\pi\xi_\parallel/a) \approx \pi/2$. If $\xi_\parallel \ll M$, we can use $\tan^{-1}(2\pi\xi_\parallel/M) \approx 2\pi\xi_\parallel/M$ to find

$$s^2 = \frac{\xi_\parallel}{4\sigma_{\mathrm{eff}}}(1 - 4\xi_\parallel/M) \qquad \xi_\parallel \ll M \tag{35}$$

while in the opposite limit one obtains a result independent of $\xi_\parallel$,

$$s^2 \approx M/[(2\pi)^2\sigma_{\mathrm{eff}}] \qquad \xi_\parallel \gg M. \tag{36}$$

Combining equations (35) and (27) one concludes

$$s^2 \propto L^2 \tag{37}$$

i.e. the width of the interfacial profile is of the same order as the thickness of the strip. For long-range forces, on the other hand, using equation (32) for $\bar{\ell} = L/2$ yields

$$\xi_\parallel \propto L^{(\delta+2)/2} \qquad s^2 \propto L^{(\delta+2)/2} < L^2 \qquad \text{for } \delta < 2. \tag{38}$$

Thus the capillary wave treatment allows a simple generalization of the results known from the exact calculations, equations (9)–(15) and (17). However, it should be noted that the validity of equation (18) has been questioned on rather general grounds [87, 88].

Finally, we discuss the scaling theory for critical wetting [45, 69] and the interface localization–delocalization transition that results from the capillary wave treatment in $d = 2$, considering both the case of short-range forces and of long-range wall potentials with $\delta = 2$. Denoting the distance from the wetting transition temperature as ε, the singular part of the free energy of the strip for small ε scales as follows

$$F_{\mathrm{sing}} = L^{-2}\tilde{F}(L\varepsilon^{\nu_\parallel/2},\ h\varepsilon^{-3\nu_\parallel/2}) = L^{-2}\tilde{F}(L\xi_\parallel^{-1/2},\ h\xi_\parallel^{3/2}). \tag{39}$$

In equation (39), we have ignored prefactors in the arguments of the scaling function $\tilde{F}(X, Y)$ for simplicity. Taking first the limit $L \to \infty$ and then the limit $\varepsilon \to 0$, the L-dependence must cancel out from equation (39), and hence F_{sing} reduces to

$$F_{\mathrm{sing}} = \varepsilon^{\nu_\parallel}\tilde{f}(h_\varepsilon^{-3\nu_\parallel/2}) = \xi_\parallel^{-1}\tilde{f}(h\xi_\parallel^{3/2}) \tag{40}$$

where $\tilde{f}(Y)$ is another scaling function.

Now the theory [69] shows that for short-range wall forces as well as for long-range wall forces with $\delta > 2$ the entropic interaction equation (28) dominates, and one finds exactly the same exponent $\nu_\parallel$ as in Abraham's exact solution [60, 72], namely $\nu_\parallel = 2$, and thus $F_{\mathrm{sing}} = \varepsilon^2\tilde{f}(h\varepsilon^{-3})$. On the other hand, if we keep L finite, F_{sing} shows (nearly) a singularity

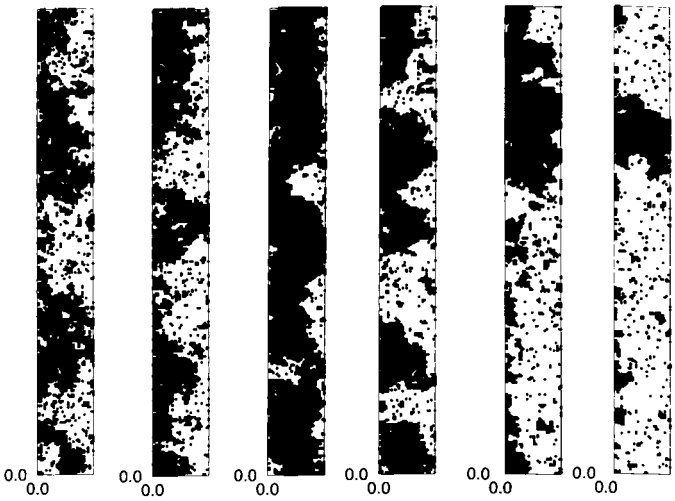

Figure 2. Snapshot of Ising strips with $L = 31$, $M = 310$, $h/J = 0.25$ for several choices of $t = T/T_c$: 1.02, 1.00, 0.98, 0.96, 0.94 and 0.92 (from left to right). Down spins are shown as black dots, up spins are not shown.

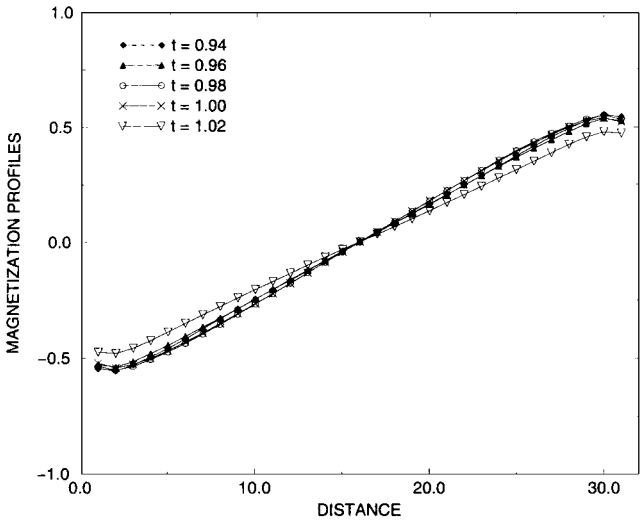

Figure 3. Magnetization profiles of Ising strips with $L = 31$, $M = 310$, $h/J = 0.25$ for several choices of $t = T/T_c$, as indicated in the figure.

when the argument X in equation (39) is unity, and this yields the interface localization transition, i.e., $\varepsilon_c(L) = [T_w - T_c(L)]/T_w$. Thus

$$X = L\varepsilon_c = 1 \qquad \varepsilon_c(L) = L^{-1} \qquad T_c(L) - T_w \propto L^{-1} \tag{41}$$

both in the short-range case [37, 44] and in the long-range case for $\delta > 2$.

Exactly for $\delta = 2$, however, which is the case that will be numerically studied in the present paper, a very interesting different behaviour occurs: F_{sing} only has an essential singularity, since the correlation length $\xi_\parallel$ diverges more strongly than any power law [69],

$$\xi_\parallel \propto \exp[\text{const} \times \varepsilon^{-1/2}]. \tag{42}$$

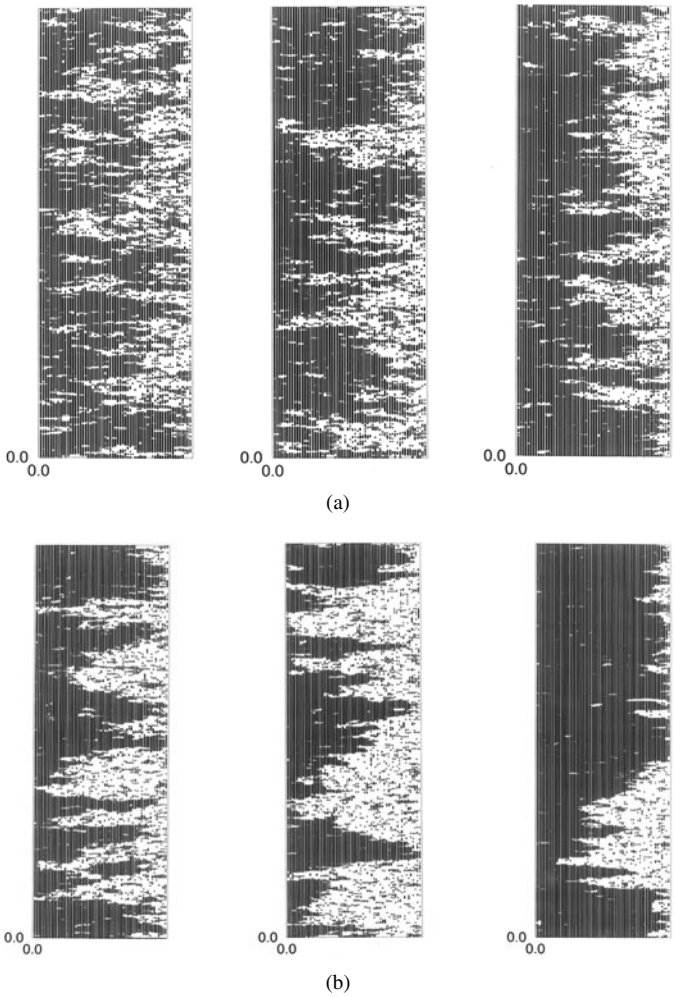

Figure 4. Snapshot of Ising strips with $L = 61$, $M = 1220$, $h/J = 0.25$ for $t = 1.04$, 1.02 and 1.00 (a), and 0.98, 0.96 and 0.94 (b). Down spins are shown as black dots, up spins are not shown.

Equation (42) is reminiscent of a Kosterlitz–Thouless transition [103]. In fact, just as in the latter problem both the enthalpy of a vortex–antivortex pair at distance ℓ scales as $J \ln \ell$ and the entropy scales as $T \ln \ell$, in the present case the enthalpy of the interface at distance ℓ from the wall scales as $-h\ell^{-2}$ and the entropy scales as $T\ell^{-2}$, equation (28), so one again has a marginal case where both energy and entropy of the relevant degree of freedom scale in the same way with the length.

Note that equation (42) formally means $\nu_\parallel = \infty$, but the last expression on the right-hand side of equations (39) and (40) can still be used. Applying again the criterion $X = 1$ (for $Y = 0$) to locate the interface localization–delocalization transition, we obtain the rather unconventional new result

$$X = L\xi_\parallel^{-1/2} = 1 \Rightarrow \xi_\parallel^c = L^2 \qquad \varepsilon_c(L) \propto (\ln L)^{-2} \tag{43}$$

i.e.,

$$T_c(L) - T_w \propto (\ln L)^{-2}. \tag{44}$$

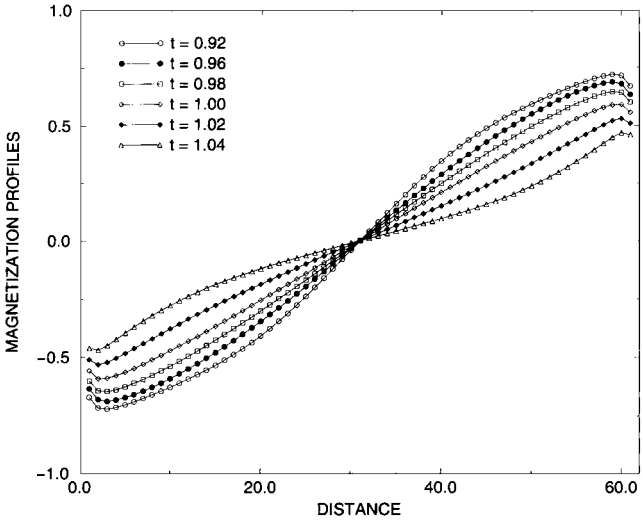

Figure 5. Magnetization profiles of Ising strips with $L = 61$, $M = 1220$, $h/J = 0.25$, $t = 1.04$, 1.02, 1.00, 0.98, 0.96 and 0.92.

This result means that now $T_c(h)$ is much more strongly depressed from T_w with decreasing L than in the short-range case (equation (41)).

3. The Ising strip with competing boundary fields $H_n \propto n^{-3}$

Monte Carlo simulations have been performed for $(L \times M)$ lattices, for the choices $L = 7$, 15, 31 and 61, respectively, and $M = 10\ L$ was chosen for $L \leqslant 31$ while $M = 20\ L = 1220$ was chosen for $L = 61$. Some runs were also performed for L as large as $L = 121$ but we found it rather difficult to obtain results of sufficient statistical accuracy for this strip width. Note that we applied a single spin-flip Metropolis algorithm [104] throughout. Since the problem involves a subtle competition between bulk and interfacial fluctuations and since, due to the boundary fields, fluctuations near the boundaries are less correlated than fluctuations in the bulk, we considered that cluster algorithms would offer little practical advantage, for the regime of sizes accessible in the present study. Note that we investigated several choices of the amplitude h of the boundary field, equation (3), namely $h/J = 0.10$, 0.25, 0.375, 0.50 and 0.65. For these choices of field amplitudes h, temperature scans were performed in order to locate the (pseudocritical) transition temperature from the maximum of the susceptibility, as done successfully in the short-range case [31–33]. The susceptibility is recorded from the fluctuations of the total magnetization $m = (LM)^{-1} \sum_i S_i$ as

$$k_B T \chi' = (LM)(\langle m^2 \rangle - \langle |m| \rangle^2). \tag{45}$$

In addition, at the reduced temperature $t \equiv T/T_c = 0.5$ we have also performed scans of h, in order to cross the curve of transition points $h_c = h_c(T)$ in a different direction than above, and thus have a check on the numerical reliability of our procedures. Since the total number of parameter combinations to be investigated was rather large, we had to be content with a relatively modest statistical effort (typically 10^6 Monte Carlo steps per lattice site were used). Even the present investigation needed a computer time investment of the order of 10^3 workstation hours.

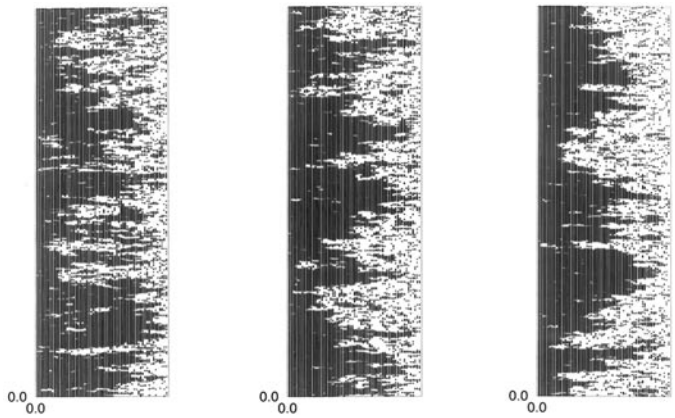

(a)

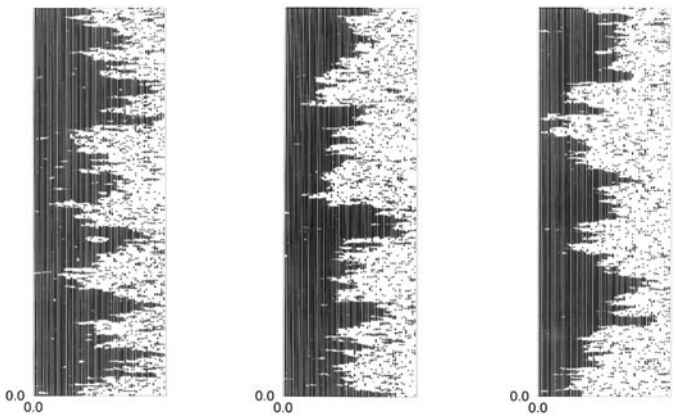

(b)

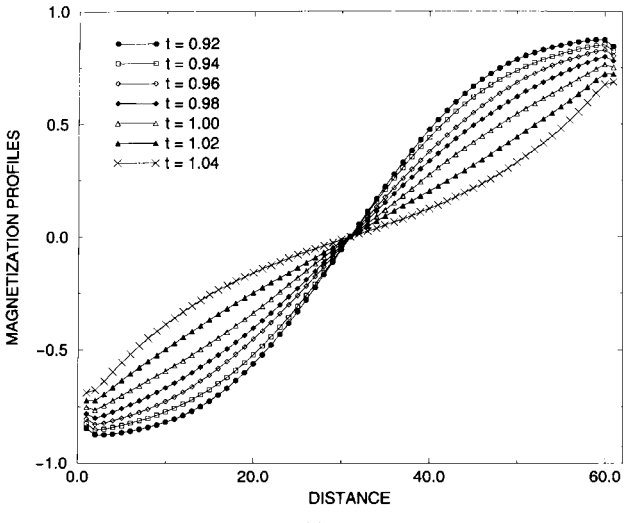

(c)

Figure 6. (a) Snapshots of Ising strips with $L = 61$, $M = 1220$, $h/J = 0.50$, $t = 1.02$, 1.00 and 0.98 (a), $t = 0.96$, 0.94 and 0.92 (b) and corresponding magnetization profiles (c).

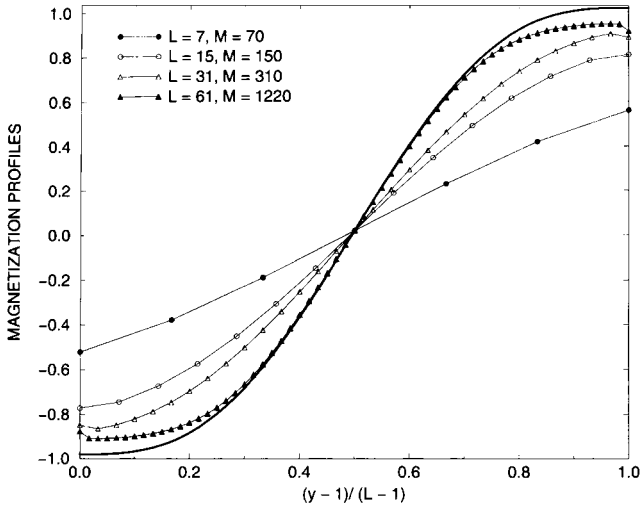

Figure 7. Comparison of magnetization profiles for $h/J = 0.5$, $t = 0.85$ and $L = 7, 15, 31$ and 61. The prediction of equation (10) is included (thick curve, the value m_b of the bulk magnetization was taken from the exact solution [104]).

Figures 2–7 present typical data for $L = 31$ and $L = 61$, both for $h = 0.25$, focusing on the magnetization profiles m_n against n across the strip, together with corresponding snapshot configurations. For $0.98 \leqslant t \leqslant 1.02$ the snapshots show the typical critical clusters, with very irregular surfaces, and many holes inside them, typical for fractal objects in the critical region. Comparing these shapshots with corresponding pictures without the long-range boundary field (cf e.g. [31, 33]), one would not be able to tell the difference. As we shall see later, the quantitative analysis of our results confirms this impression that the long-range boundary field produces very similar effects to its short-range counterpart, very unlike the three-dimensional case [97].

For $T < T_c$ but $T > T_w(h)$ one can see very clearly that the wandering interface explores the whole strip, consistent with the theoretical ideas reviewed in the previous section (note that the scale in the x-direction has been strongly compressed for $L = 61$). The state for $L = 61$, $t = 0.94$ is a nice example for a state at $T < T_w(h)$, with a symmetry-broken state of positive overall magnetization in the strip. This case (as well as the corresponding profile) indicates that the domain size $\ell_{\text{domain}} \propto \exp(\text{const} \times L)$ mentioned above exceeds $M = 1220$ already distinctly, and so we have a monodomain sample rather than a multidomain configuration. In contrast, the snapshot picture at $t = 0.96$ could be interpreted as a configuration with two domains present, a domain with positive magnetization in the rest, but also inside these domains the interface is still wandering a distance comparable to the width of the strip, and in fact this temperature is estimated to be rather close to $T_c(h, L = 61)$. In any case, the snapshots confirm the qualitative assertion of figure 1(a) that overhangs as well as 'bubbles and holes' are present.

The magnetization profiles give clear evidence that the width of the profile always is of the same order as the widths of the strip, consistent with the theoretical considerations of the previous section. An interesting feature is that for large L (e.g. $L = 61$) the maximum of $|m_n|$ does not occur for $n = 1$ or $n = L$ but somewhat away from the boundary, inside the strip. This effect is observed both for $T = T_c$ and for $T < T_c$, and for all choices of h (including $h/J = 0.50$, see figure 6).

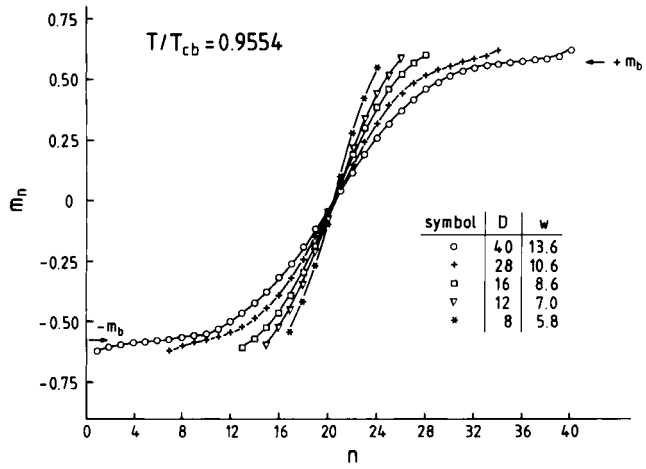

(a)

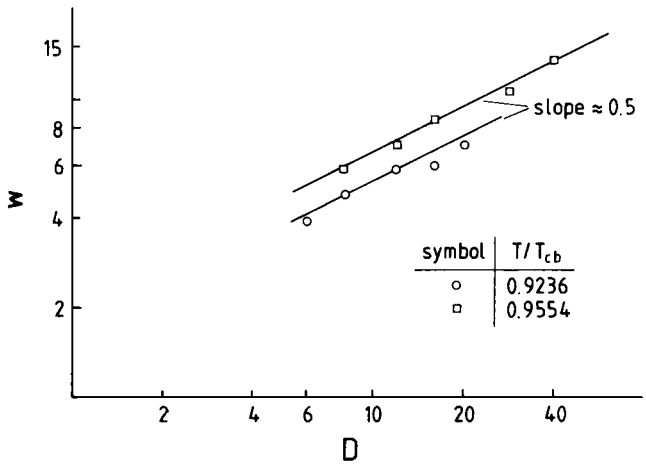

(b)

Figure 8. (a) Comparison of magnetization profiles for the three-dimensional simple cubic Ising ferromagnet at $J/k_BT = 0.232$ ($T/T_{cb} = 0.9554$) and thin films of thickness $D = 8$ up to $D = 40$, as shown in the figure, for the choice of short-range boundary fields, equation (3), with $h/J = 0.55$. Data were generated in [52]. Arrows indicate that flat plateaus soon develop at the bulk magnetization m_b. (b) A log–log plot of the widths w (defined here from $w = 2m_b/(\mathrm{d}m/\mathrm{d}z)_0$ where $(\mathrm{d}m/\mathrm{d}z)_0$ is the slope of the profile at the midpoint, $m(z) = 0$) versus film thickness D. From Kerle *et al* [106].

In the three-dimensional Ising model no evidence for such an effect was found (figure 8). It is also obvious that the shape of the magnetization profiles in $d = 2$ (figure 7) and $d = 3$ (figure 8) differ qualitatively: in $d = 3$ for film thickness $D \to \infty$ the magnetization profile as a function of the normalized variable $z = y/D$ simply develops into a step-function for $T > T_c(h, D)$, since the width only scales as $w \propto \sqrt{D}$ for short-range wall forces [96, 105] and as $w \propto \ell \ln D$ for long-range wall forces [97],

$$m(z) = m_b[-1 + 2\theta(z - \tfrac{1}{2})] \qquad D \to \infty \qquad T_w(h) < T < T_c. \tag{46}$$

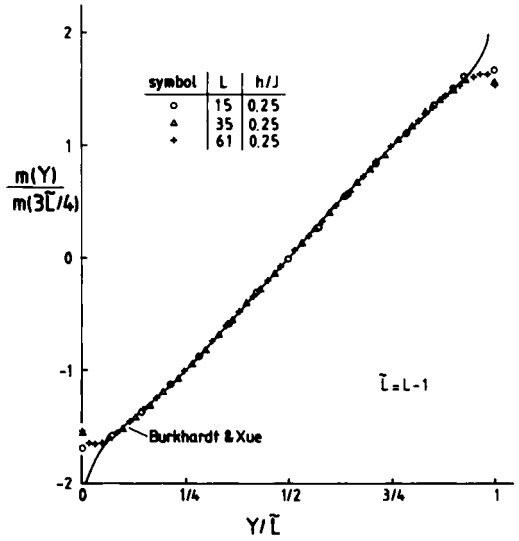

Figure 9. Normalized magnetization profiles $m(y)/m(3\tilde{L}/4)$ plotted against $y/\tilde{L}$ ($\tilde{L} = L - 1$) right at T_c for several choices of L as indicated in the figure. The full curve is the theoretical prediction by Burkhardt and Xue [40], equation (15).

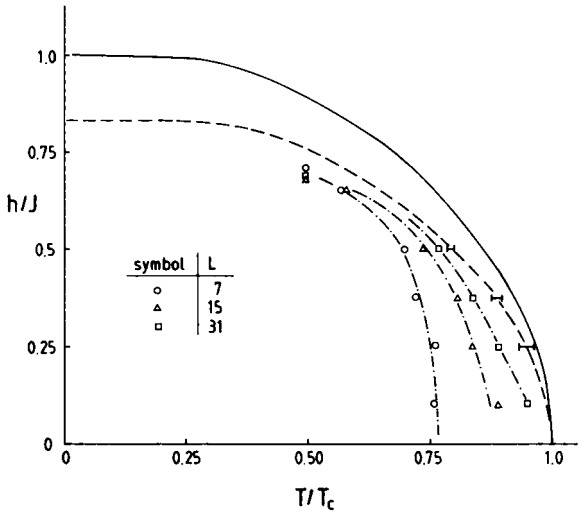

Figure 10. Location of the interface localization–delocalization transition temperature $T_c(h)$ for various choices of h and L, as indicated in the figure. The temperature is measured in units of the bulk critical temperature known from the exact solution [105]. All Monte Carlo data refer to the choice of the long-range potential, equation (4). The broken curve is a tentative extrapolation (cf figure 11) to $L \to \infty$. The limiting field $h_c(T \to 0) = [\sum_{n=1}^{\infty} n^{-3}]^{-1}$ is known exactly, of course. For comparison, also the exact result for the short-range case, equation (3), due to Abraham [60], equation (16), has been included as a full curve.

In contrast, for $d = 2$ the width w of the profile and the strip width L scale proportionally to each other, and therefore in the limit $L \to \infty$ a nontrivial profile results, predicted from the SOS model by equation (10), and confirmed by the capillary wave approach.

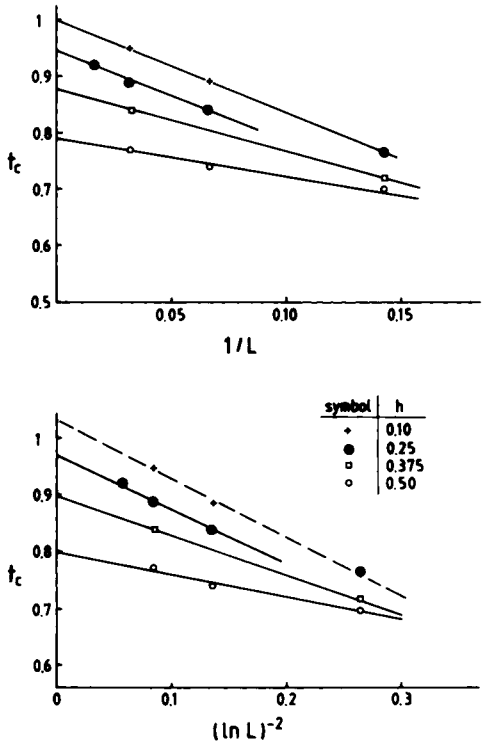

Figure 11. Extrapolation of $T_c(h)$ against $1/L$ (upper part) and against $(\ln L)^{-2}$ (lower part), for several choices of h as indicated in the figure. Temperature T is measured in units of the bulk critical temperature, $t_c \equiv T_c(h)/T_{cb}$. Dashed straight lines indicate extrapolations which are physically implausible (see text).

While the magnetization profile indeed is a straight line in its central part at all temperatures near T_c and below, we do not find any clear evidence that the results converge against a simple straight line over the full width of the strip at $T_c(h, L)$ as $L \to \infty$, as predicted in equation (17). It is unclear to us whether this problem reflects the possibility that equation (17) does not hold for the long-range potential considered here, equation (3), or whether our strip widths L are not yet large enough, or whether the statistical errors of our data simply are underestimated. A substantially larger computational effort, not yet possible at present, would be needed to clarify that problem.

It is also interesting to compare our profiles right at the bulk critical temperature, T_{cb}, to test the prediction by Burkhardt and Xue [40]. As is obvious from figure 9, the theoretical curve (equation (15)) is very close to a straight line (from $0.1 \leqslant y/L \leqslant 0.9$) and significant deviations occur only near $y/L \to 0$ and $y/L \to 1$ where $m(y) \to \pm\infty$. Since the slope of the straight line is essentially fixed by the chosen normalization of the ordinate, it is not clear whether the good agreement between simulation data and theory is significant: as a matter of fact, the simulations bend over both at $y/L \to 0$ and $y/L \to 1$, and show no evidence for the predicted divergence of equation (15) yet. Of course, $m(y)$ must be finite at layer $n = 1$ and $n = L$ for any finite L, and thus it is a subtle matter how this singular behaviour develops in the thermodynamic limit.

Next we turn to our results for the interface localization–delocalization transition (figures 10 and 11). One recognizes that the phase diagrams resemble the phase diagrams

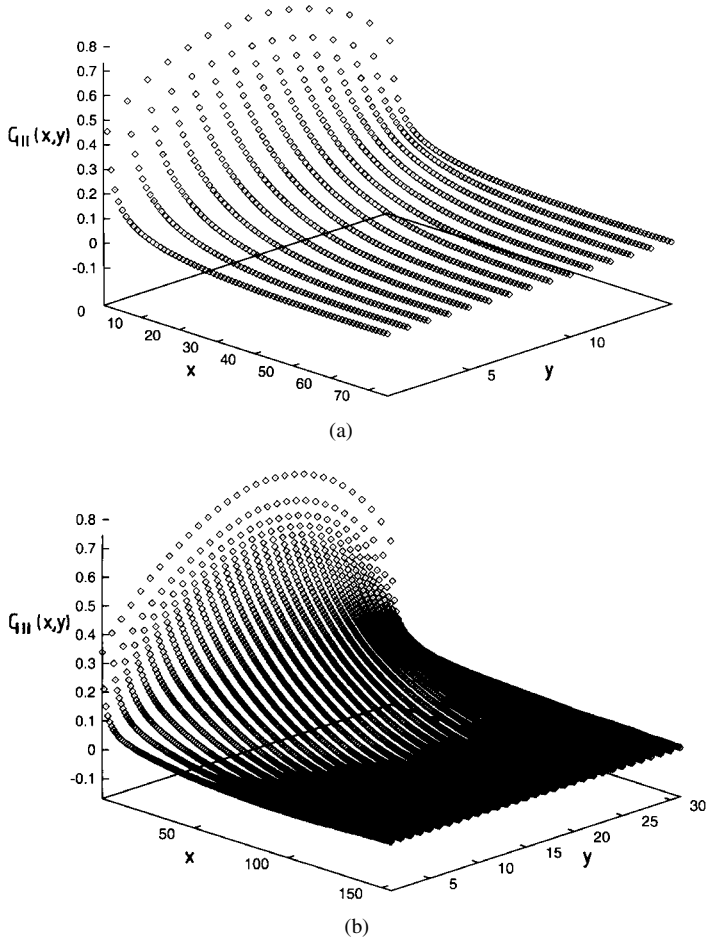

Figure 12. Correlation function $G_{\parallel}(x, y)$ for the choice of parameters $h/J = 0.25$, $t = 0.94$ and $L = 15$ (a) or $L = 31$ (b), respectively.

that apply in the case with short-range interaction [31, 60]. Of course, the extrapolation to the thermodynamic limit $L \to \infty$ is somewhat uncertain, in particular in the vicinity of the bulk critical temperature T_{cb}: the treatment of section 2.3 in terms of the capillary wave Hamiltonian makes sense only for strip widths L which are far larger than the correlation length ξ_b of bulk thermal fluctuations. Clearly, for strips as narrow as $L = 7$ and temperatures $t \geqslant 0.9$ this condition is not met. As a result, for small fields ($h = 0.25$) where the critical temperatures $t_c(L)$ for $L \geqslant 15$ are so close to unity, one expects a crossover from the anisotropic finite-size scaling of equation (39), where L scales with $\xi_{\perp} \propto \xi_{\parallel}^{1/2}$, to the standard isotropic finite-size scaling where L scales with ξ_b [107–109]. Thus it is clear that the extrapolation based on equation (44) does not work for small h—indeed the extrapolated wetting transition temperature $T_w = T_{cb}t_c(\infty)$ would exceed T_{cb}, which is physically implausible. Probably the data for $h = 0.1$ fall mostly in the region where bulk finite-size scaling holds, while for $h = 0.25$ the irregular behaviour may indicate crossover effects. Unfortunately, even for $h = 0.375$ and $h = 0.5$ our results cannot really distinguish between the short-range result, equation (41), and the new prediction, equation (44): both possibilities lead to equally well

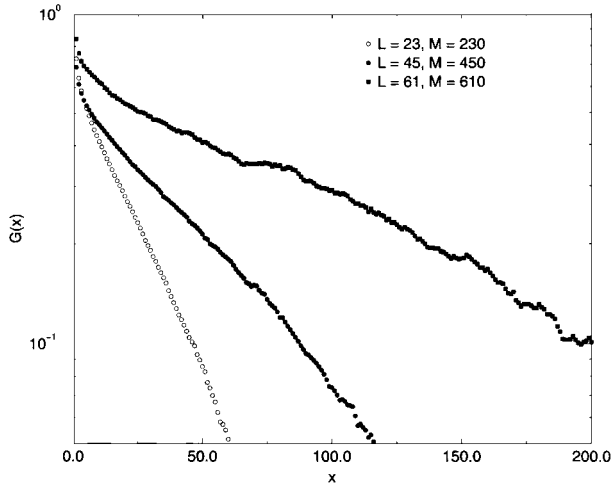

(a)

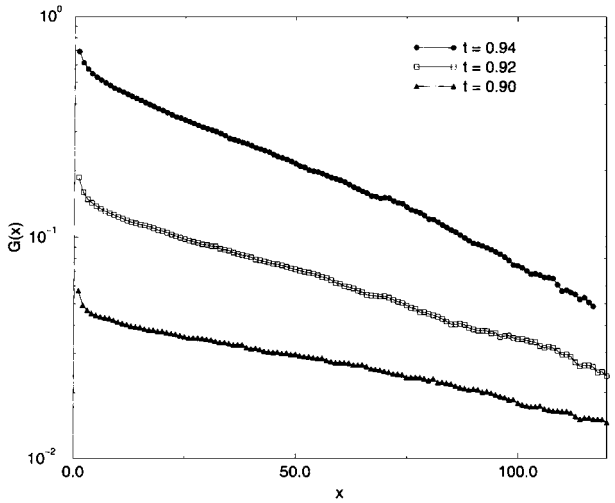

(b)

Figure 13. Semilog plot of the correlation function $G(x) \equiv G_{\parallel}(x, y = (L+1)/2)$ in the centre of the film versus x. Case (a) refers to the choice of parameters $t = 0.94$, $h/J = 0.25$ and three choices of (L, M) as indicated in the figure; case (b) refers to the choice $L = 45$, $M = 450$, $h/J = 0.25$ and three choices of the reduced temperature t, as shown in the figure.

defined straight lines, and also the predictions for T_w $(= T_{cb}t_c(\infty))$ would not be very different from each other, as the comparison of the lower and upper part of figure 11 demonstrates. As one usually finds with logarithmic laws such as equation (44), a much wider range of L would be necessary in order to clearly establish that equation (44) rather than equation (41) holds, and this is not possible at present.

We now turn to the behaviour of the correlation function $G_{\parallel}(x, y)$ (equation (7)) and associated correlation length $\xi_{\parallel}$, see figures 12 and 13. All these data refer to the temperature regime between the interface localization–delocalization transition $T_c(L)$ and the bulk critical temperature. As a consequence, $G_{\parallel}(x, y)$ reaches rather large values for short distances x ($x = 1, 2$, for instance), and is maximal in the middle of the film ($y = (L+1)/2$).

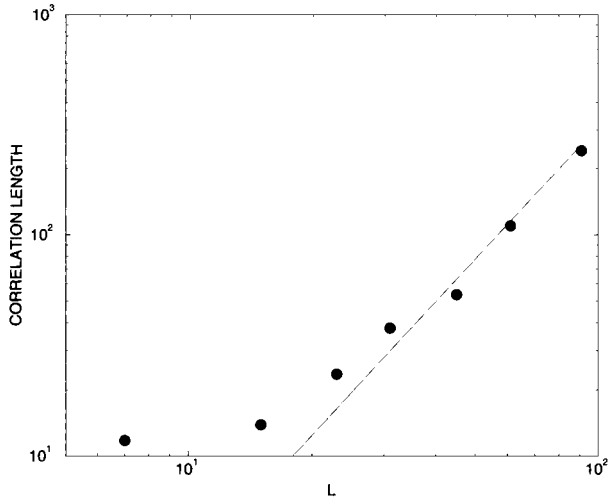

Figure 14. Log–log plot of $\xi_{\parallel}$ against L for $t = 0.94$ and $h/J = 0.25$.

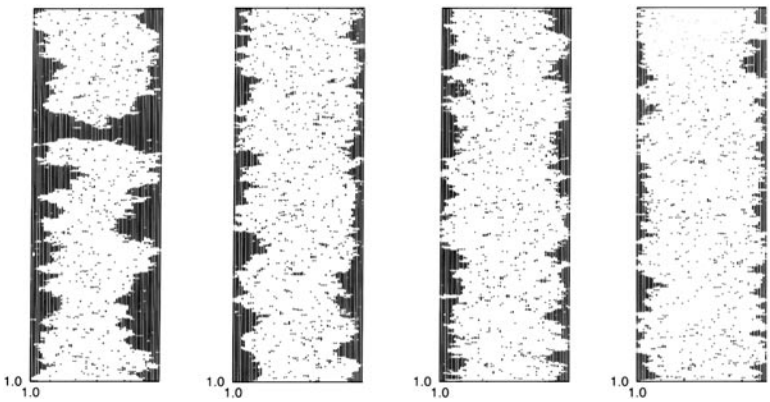

Figure 15. Snapshots of Ising strips with $L = 61$, $M = 610$, $h/J = 0.60$ and $t = 0.85$, for four choices of the bulk field: $H/J = -0.05, -0.10, -0.15$ and -0.20 (from left to right, respectively). Note that spin down is interpreted as gas, spin up as liquid and occupied sites are indicated by a dot.

A qualitatively similar behaviour has already been seen in a study of $G_{\parallel}(x, y)$ for a three-dimensional model of a confined binary polymer mixture [96]. In that case, however, the maximum of $G_{\parallel}(x, y)$ as a function of y was much sharper, in particular for large x, so $G_{\parallel}(x, y)$ essentially behaved as a slowly decaying ridge centred at $y = (L+1)/2$, while a few lattice spacings away from the centre the correlation function decays to zero with increasing x very fast. In fact, for $d = 3$ dimensions and the short-range boundary fields considered there [96], one expects an exponential variation of the correlation lengths $\xi_{\parallel}$ with the thickness L of the film, unlike the power law variation expected for the present case (see section 2). This is qualitatively consistent with figures 12(a), (b), when we compare the case $L = 15$ with the case $L = 31$ (note the different scales for x, however).

For a more quantitative analysis we fit the correlation function $G(x) \equiv G_{\parallel}(x, y = (L+1)/2))$ in the centre of the film (figure 13) to a simple exponential decay, $G(x) \propto \exp(-x/\xi_{\parallel})$.

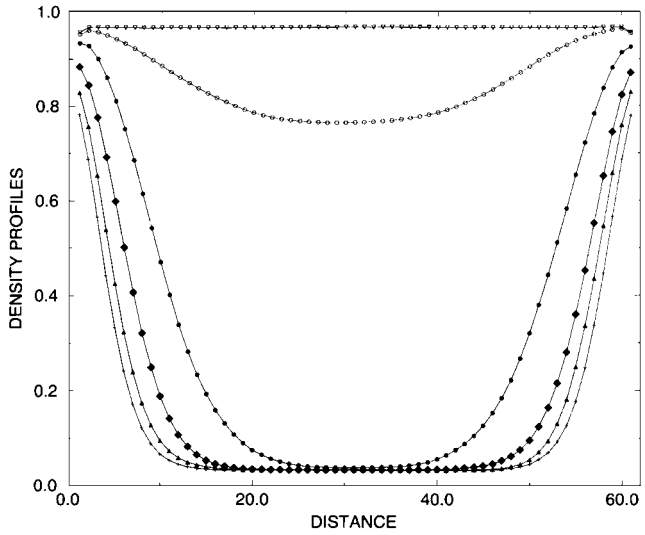

Figure 16. Density profiles $\rho(n)$ plotted against distance n across the film with $L = 61$, $M = 610$, $t = 0.85$, $h/J = 0.60$ and several choices of the bulk field: $H = 0$ (open triangles), $H/J = -0.000\,25$ (open circles), $H/J = -0.005$ (full dots), $H/J = -0.010$ (diamonds), $H/J = -0.015$ (full triangles), $H/J = -0.020$ (crosses), respectively.

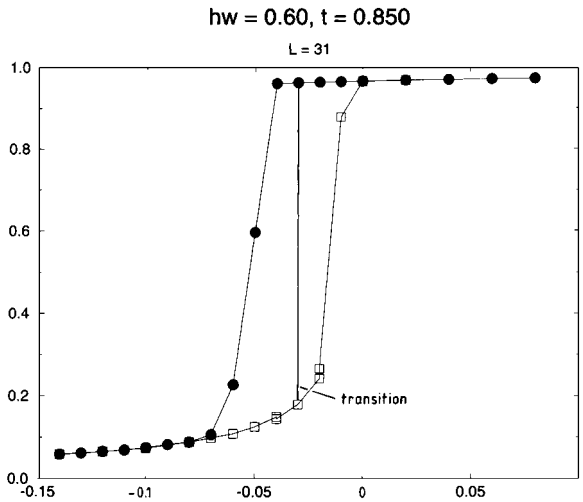

Figure 17. Plot of the total density ρ against the bulk field H/J, for the case $L = 31$, $M = 310$, $t = 0.85$ and $h/J = 0.60$. Full dots refer to a choice of the initial state with $\rho = 1$, while open squares refer to a choice of the initial state with $\rho = 0$. Thermodynamic integration yields a location of the transition at $H/J \approx -0.032$.

This fitting procedure is subtle, since there are systematic deviations for small x, where this asymptotic law is not yet expected to hold, as well as for large x; the latter are probably due to insufficient equilibration and to finite size effects (M might have been not large enough). At $t = 0.94$, we restricted the fit to the range $0.15 \leqslant G(x) \leqslant 0.50$ (after checking that a slightly different choice of this fitting interval yielded similar results). The correlation length $\xi_{\parallel}$ estimated in this way is plotted against L in figure 14 on a log–log plot. For large L these

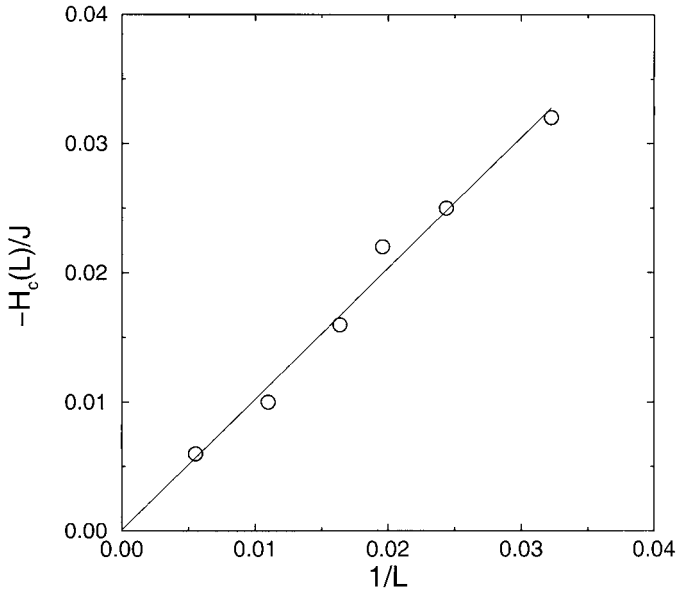

Figure 18. Plot of $-H_c/J$ versus $1/L$ for $h/J = 0.60$ and $t = 0.85$, for the long-range case (open circles) and a fit with the Kelvin equation (solid line).

results are compatible with the expected behaviour $\xi_{\parallel} \propto L^2$. Note that the saturation of $\xi_{\parallel}$ for small L is expected, since $\xi_{\parallel}$ should not fall below ξ_b (note $\xi_b(t = 0.94) \approx 4.73$).

In summary, hence, we have seen that Ising strips with competing boundary fields (decaying with distance n as $\pm n^{-3}$) behave qualitatively very similarly to the case of short-range boundary fields. Our simulation data are compatible with the pertinent theoretical predictions, although a substantially better accuracy and a much wider range of L clearly would be desirable—but this does not seem feasible at present.

4. Capillary condensation with long-range boundary fields

We now describe our results for the alternative choice of boundary fields, equation (5), which have the same sign rather than opposite signs, but include now a bulk field $H < 0$ in order to be able to observe a phase transition between a state of positive magnetization (for $H > H_c$) to negative magnetization (for $H < H_c < 0$). While for $L \to \infty$ this transition occurs for $H_c = 0$, for finite L we expect a shift of this transition to a nonzero value $H_c(L)$. It again turns out that the behaviour of our model is rather similar to the case of short range boundary fields studied previously [30, 56], and hence we summarize our results rather briefly.

Figure 15 shows a series of snapshot pictures of the case $L = 61$ (only the phase with negative magnetization in the film is shown), while figure 16 presents corresponding density profiles (interpreting spin down as gas and spin up as liquid in a lattice gas interpretation, respectively). As in the short-range case [56], the fluctuation in the thickness of the wetting layers at the walls is of the same order as the average thickness itself, and hence well defined interfaces separating liquid and gas and running all the way parallel to the boundaries can hardly be identified—the fluid layers at the boundaries rather decompose into irregular rows of droplets attached to the boundaries. Recording the total density in the strip as a function of H/J, one recognizes that there occurs considerable hysteresis (figure 17), and hence the

(strongly first-order) capillary condensation transition must be located by the intersection of the two branches of the appropriate thermodynamic potential, as explained in [56] in detail. These thermodynamic potentials are obtained by thermodynamic integration (see [56]). We have varied the width L of the strip from $L = 31$ up to $L = 181$ and found that the data are again reasonably well consistent with the Kelvin equation $H_c/J \propto 1/L$, as in the short-range case (figure 18) [56]. Again the accuracy of our results is not good enough to allow a reasonable search for the effects of systematic deviations from the Kelvin equation.

5. Conclusions

In this paper, Ising strips on the square lattice with nearest-neighbour ferromagnetic interaction but long-range boundary fields (of the type $\pm h/n^3$) were studied, comparing the results to corresponding studies with short range boundary fields, and to pertinent theoretical predictions.

In the case of competing boundary fields (i.e., opposite in sign but equal in absolute strength) we present evidence that the interface stabilized in the system by this geometry makes excursions in its local position spanning the full width of the strip. Both at the bulk critical temperature T_{cb} and below it (not above the wetting transition temperature) the results for the profiles of the order parameter across the strip seem to converge towards the universal shapes predicted for the case of short-range boundary fields (figures 7 and 9, respectively). While we have argued that the interface localization–delocalization transition is shifted away from the wetting transition temperature T_w according to the rather unconventional law $T_w - T_c(L) \propto (\ln L)^{-2}$, unlike the short-range case where $T_w - T_c(L) \propto L^{-1}$, our data unfortunately do not allow us to distinguish between these two possibilities (figures 10 and 11). The correlation function $G_{\parallel}(x, y)$ also has been studied and preliminary estimates for the associated correlation length $\xi_{\parallel}$ have been obtained as well, and found to be compatible with the theoretical expectations.

Finally, for the case where both boundary fields have the same sign, capillary condensation phenomena are found to occur which again resemble very strongly the corresponding behaviour for the short-range case. Thus we feel that all these phenomena are of a fairly general character, thus are not sensitive to specific details of the models that have been studied. It hence would be very interesting to look for such phenomena in corresponding experiments on monolayers adsorbed on stepped surfaces.

Acknowledgment

This research was supported in part by the Volkswagenstiftung, grant No I/74168.

References

[1] Binder K and Hohenberg P C 1972 *Phys. Rev.* B **6** 3461
[2] Nicholson D 1975 *J. Chem. Soc. Faraday Trans.* I **71** 238
[3] Au-Yang H and Fisher M E 1975 *Phys. Rev.* B **11** 3469
[4] Fisher M E and DeGennes P G 1978 *C. R. Acad. Sci. Paris* **287** 207
[5] Fisher M E and Au-Yang H 1980 *Physica* A **101** 255
[6] Au-Yang H and Fisher M E 1980 *Phys. Rev.* B **21** 3956
[7] Abraham D B and Issyeoni M E 1980 *J. Phys. A: Math. Gen.* **13** L89
[8] Fisher M E and Nakanishi H 1981 *J. Chem. Phys.* **75** 1981
[9] Abraham D B 1982 *Phys. Rev.* B **25** 4922
[10] Nakanishi H and Fisher M E 1983 *J. Chem. Phys.* **78** 3279
[11] Abraham D B 1983 *Phys. Rev. Lett.* **50** 297

[12] Evans R and Taranzona P 1984 *Phys. Rev. Lett.* **52** 557
[13] Lipowsky R and Gompper G 1984 *Phys. Rev.* B **29** 5213
[14] Abraham D B 1984 *Phys. Rev.* B **29** 525
[15] Privman V P and Fisher M E 1984 *Phys. Rev.* B **30** 322
[16] Sornette D 1985 *Phys. Rev.* B **31** 4672
[17] Evans R and Marini Bettolo Marconi U 1985 *Chem. Phys. Lett.* **114** 415
[18] Evans R, Marini Bettolo Marconi U and Taranzona P 1986 *J. Chem. Soc. Faraday Trans.* II **82** 1763
[19] Stecki J, Ciach A and Dudowicz J 1986 *Phys. Rev. Lett.* **56** 1482
[20] Evans R, Marini Bettolo Marconi U and Taranzona P 1987 *J. Chem. Phys.* **86** 7138
[21] Bruno E, Marini Bettolo Marconi U and Evans R 1987 *Physica* A **141** 187
[22] Peterson B K and Gubbins K E 1987 *Mol. Phys.* **62** 215
[23] Heffelfinger G S, van Swol F and Gubbins K E 1987 *Mol. Phys.* **61** 1381
[24] Panagiotopoulos A Z 1987 *Mol. Phys.* **62** 701
[25] Peterson B K, Gubbins K E, Heffelfinger G S, Marini Bettolo Marconi U and van Swol F 1988 *J. Chem. Phys.* **88** 6487
[26] Desideri J-P and Sornette D 1988 *J. Physique* **49** 1411
[27] Privman V and Švrakić N M 1988 *Phys. Rev.* B **37** 3713
[28] Walton J P R B and Quirke N 1989 *Mol. Simul.* **2** 361
[29] Nicolaides D and Evans R 1989 *Phys. Rev.* B **9** 9336
[30] Albano E V, Binder K, Heermann D W and Paul W 1989 *J. Chem. Phys.* **91** 3700
[31] Albano E V, Binder K, Heermann D W and Paul W 1989 *Surf. Sci.* **223** 151
[32] Kroll D M and Gompper G 1989 *Phys. Rev.* B **99** 433i
[33] Albano E V, Binder K, Heermann D W and Paul W 1990 *J. Stat. Phys.* **61** 161
[34] Liu A J, Durian D J, Herbholzheimer E and Safran S A 1990 *Phys. Rev. Lett.* **65** 1897
[35] Parry A O and Evans R 1990 *Phys. Rev. Lett.* **64** 439
[36] Evans R 1990 *J. Phys.: Condens. Matter* **2** 8989
[37] Parry A O, Evans R and Nicolaides D B 1991 *Phys. Rev. Lett.* **67** 2978
[38] Swift M R, Owczarek A L and Indekeu 1991 *Europhys. Lett.* **14** 475
[39] Liu A J and Grest G S 1991 *Phys. Rev.* A **44** R7894
[40] Burkhardt T W and Xue T 1991 *Phys. Rev. Lett.* **66** 895
[41] Binder K and Landau D P 1992 *J. Chem. Phys.* **96** 1444
[42] Binder K 1992 *Annu. Rev. Phys. Chem.* **43** 33
[43] Parry A O and Evans R 1992 *J. Phys. A: Math. Gen.* **25** 275
[44] Parry A O and Evans R 1992 *Physica* A **181** 250
[45] Parry A O 1992 *J. Phys. A: Math. Gen.* **25** 257
[46] Eisenregler E, Krech M and Dietrich S 1993 *Phys. Rev. Lett.* **70** 619
[47] Stecki J 1993 *Phys. Rev.* B **47** 7519
[48] Stecki J, Maciolek A and Olausen K 1994 *Phys. Rev.* B **49** 1092
[49] Evans R and Stecki J 1994 *Phys. Rev.* B **49** 8842
[50] Binder K, Ferrenberg A M and Landau D P 1994 *Ber. Bunsenges. Phys. Chem.* **98** 340
[51] Binder K, Landau D P and Ferrenberg A M 1995 *Phys. Rev. Lett.* **74** 298
[52] Binder K, Landau D P and Ferrenberg A M 1995 *Phys. Rev. Lett.* E **51** 2823
[53] Binder K, Evans R, Landau D P and Ferrenberg A M 1996 *Phys. Rev.* E **53** 5023
[54] Maciolek A 1996 *J. Phys. A: Math. Gen.* **39** 3837
Maciolek A and Stecki J 1996 *Phys. Rev.* B **54** 1128
[55] Parry A O, Boulter C J and Swain P S 1995 *Phys. Rev.* E **52** 5768
[56] Albano E V, Binder K and Paul W 1997 *J. Phys. A: Math. Gen.* **30** 3285
[57] Ferrenberg A M, Landau D P and Binder K 1998 *Phys. Rev.* E **58** 3353
[58] Cahn J W 1977 *J. Chem. Phys.* **66** 3667
[59] Ebner C and Saam W F 1977 *Phys. Rev. Lett.* **38** 1486
[60] Abraham D B 1980 *Phys. Rev. Lett.* **44** 1165
[61] van Leeuwn J M J and Hilhorst H J 1981 *Physica* A **107** 319
[62] Chui S T and Weeks J D 1981 *Phys. Rev.* B **23** 2438
[63] Burkhardt T W 1981 *J. Phys. A: Math. Gen.* **14** L63
[64] Nakanishi H and Fisher M E 1982 *Phys. Rev. Lett.* **49** 1565
[65] Knoll D M and Lipowsky R 1983 *Phys. Rev.* B **28** 5273
[66] Lipowsky R, Knoll D M and Zia R K P 1983 *Phys. Rev.* B **27** 4499
[67] Brezin E, Halperin B I and Leibler S 1983 *Phys. Rev. Lett.* **50** 1387

[68] Fisher M E 1984 *J. Stat. Phys.* **34** 667
[69] Fisher D S and Huse D A 1985 *Phys. Rev.* B **32** 247
[70] Kroll D M, Lipowsky R and Zia R K P 1985 *Phys. Rev.* B **32** 1862
[71] deGennes P G 1985 *Rev. Mod. Phys.* **57** 827
[72] Abraham D B and Smith E R 1986 *J. Stat. Phys.* **43** 621
[73] Fisher M E 1986 *J. Chem. Soc. Faraday Trans.* II **82** 1569
[74] Sullivan D E and Telo da Gama M M 1986 *Fluid Interfacial Phenomena* ed C A Croxton (New York: Wiley) p 45
[75] Binder K, Landau D P and Knoll D M 1986 *Phys. Rev. Lett.* **56** 2272
[76] Lipowsky R and Fisher M E 1987 *Phys. Rev.* B **36** 2126
[77] Binder K and Landau D P 1988 *Phys. Rev.* B **37** 1745
[78] Abraham D B 1988 *J. Phys. A: Math. Gen.* **21** 1741
[79] Dietrich S 1988 *Phase Transitions and Critical Phenomena* vol 12, ed C Domb and J L Lebowitz (London: Academic) p 1
[80] Abraham D B and Huse D A 1988 *Phys. Rev.* B **38** 7169
[81] Privman V and Švrakić N M 1988 *Phys. Rev.* B **37** 5974
[82] Burkhardt T W 1989 *Phys. Rev.* B **40** 6987
[83] Binder K, Landau D P and Wansleben S 1989 *Phys. Rev.* B **40** 6971
[84] Schick M *Liquids at Interfaces* ed J Charvolin, J F Joanny and J Zinn-Justin (Amsterdam: North-Holland) p 415
[85] Jin A J and Fisher M E 1993 *Phys. Rev.* B **47** 7365
[86] Fisher M E, Jin A J and Parry A O 1994 *Ber. Bunsenges. Phys. Chem.* **98** 357
[87] Parry A O and Boulter C J 1995 *Physica* A **218** 77
[88] Boulter C J and Parry A O 1995 *Physica* A **218** 109
[89] Parry A O 1991 *J. Phys. A: Math. Gen.* **24** 1335
[90] Buff F P, Lovett R A and Stillinger F H 1965 *Phys. Rev. Lett.* **15** 621
[91] Abraham D B and Reed P 1974 *Phys. Rev. Lett.* **33** 377
[92] Weeks J D 1977 *J. Chem. Phys.* **67** 3106
[93] Abraham D B and Reed P 1974 *Phys. Rev. Lett.* **47** 545
[94] Bedeaux D and Weeks J D 1985 *J. Chem. Phys.* **82** 872
[95] Jasnow D 1984 *Rep. Prog. Phys.* **47** 1059
[96] Werner A, Schmid F, Müller M and Binder K 1997 *J. Chem. Phys.* **107** 8175
[97] Werner A, Schmid F, Müller M and Binder K 1999 *J. Chem. Phys.* **110** 1221
[98] Werner A, Schmid F, Müller M and Binder K 1999 *Phys. Rev.* E **59** 728
[99] Ciach A 1986 *Phys. Rev.* B **34** 1932
[100] Abraham D B and Martin-Löf A 1973 *Commun. Math. Phys.* **32** 245
[101] Upton P J 1999 *Phys. Rev.* E **60** R3475
[102] Fisher M E 1969 *J. Phys. Soc. Japan Suppl.* **26** 87
[103] Kosterlitz J M and Thouless D J 1973 *J. Phys. C: Solid State Phys.* **6** 1181
[104] Binder K and Heermann D W 1988 *Monte Carlo Simulation in Statistical Physics: an Introduction* (Berlin: Springer)
[105] Baxter R J 1982 *Exactly Solved Models in Statistical Mechanics* (London: Academic)
[106] Kerle T, Klein J and Binder K 1996 *Phys. Rev. Lett.* **77** 1318
[107] Fisher M E 1971 *Critical Phenomena, Proc. 1970 E Fermi Int. School Phys.* ed M S Green (London: Academic) p 1
[108] Privman V (ed) 1990 *Finite Size Scaling and Numerical Simulation of Statistical Systems* (Singapore: World Scientific)
[109] Binder K 1992 *Computational Methods in Field Theory* ed H Gausterer and C B Lang (Berlin: Springer) p 59